2009

Comparison of n-type Gd_2O_3 and Gd-doped HfO_2

Yaroslav B. Losovyj
Louisiana State University at Baton Rouge, ylozovyy@indiana.edu

David Wooten
Air Force Institute of Technology, 2950 HobsonWay, Wright Patterson Air Force Base, OH

Juan Colon Santana
University of Nebraska-Lincoln

Joonhee Michael An
University of Nebraska-Lincoln

Kirill D. Belashchenko
University of Nebraska-Lincoln, belashchenko@unl.edu

See next page for additional authors

J. Phys.: Condens. Matter **21** (2009) 045602 (8pp) doi:10.1088/0953-8984/21/4/045602

Comparison of n-type Gd_2O_3 and Gd-doped HfO_2

Ya B Losovyj[1,2], David Wooten[3], Juan Colon Santana[1], Joonhee Michael An[1], K D Belashchenko[1], N Lozova[2], J Petrosky[3], A Sokolov[1], Jinke Tang[4], Wendong Wang[4], Navamoney Arulsamy[5] and P A Dowben[1]

[1] Department of Physics and Astronomy and the Nebraska Center for Materials and Nanoscience, University of Nebraska-Lincoln, PO Box 880111, Lincoln, NE 68588-0111, USA
[2] Center for Advanced Microstructures and Devices, Louisiana State University, 6980 Jefferson Highway, Baton Rouge, LA 70806, USA
[3] Air Force Institute of Technology, 2950 Hobson Way, Wright Patterson Air Force Base, OH 45433-7765, USA
[4] Department of Physics and Astronomy, University of Wyoming, Laramie, WY 82071, USA
[5] Department of Chemistry, University of Wyoming, Laramie, WY 82071, USA

Received 18 November 2008
Published 8 January 2009
Online at stacks.iop.org/JPhysCM/21/045602

Abstract
Gd_2O_3 and Gd-doped HfO_2 films were deposited on p-type silicon substrates in a reducing atmosphere. Gd 4f photoexcitation peaks at roughly 7 and 5 eV below the valence band maximum have been identified using the resonant photoemission of Gd_2O_3 and Gd-doped HfO_2 films, respectively. In the case of Gd_2O_3, strong hybridization with the O 2p band is demonstrated, and there is evidence that the Gd 4f weighted band exhibits dispersion in the bulk band structure. The rectifying (diode-like) properties of Gd-doped HfO_2–silicon and Gd_2O_3–silicon heterojunctions are demonstrated.

1. Introduction

The position of the 4f Gd states and the extent of their hybridization is an issue for compound 4f and 5f semiconductors. In the more localized rare earth compounds, Olson *et al* [1] found evidence for 4f delocalization in $CeSb_2$, in the form of dispersing Bloch states, while 4f dispersion has been observed in other Ce [2, 3] and Yb [4] compounds. Of course f shell delocalization in metallic systems can also occur, but is more expected for the 5f levels, and Joyce and Durakiewicz, and their colleagues [5–9] and others [10] also found clear evidence of dispersion in the uranium 5f levels in uranium and uranium compounds. In the Gd^{3+} and mixed valence systems, Gd 4f hybridization with nearest neighbor atoms is expected [11, 12] and observed. In ErAs(100), strong 4f hybridization is implicated, and a direct confirmation of an occupied 4f band structure might be inferred from the data but could not established [13, 14].

We have compared the occupied density of states for Gd-doped HfO_2 for various levels of Gd doping, observing changes that could be attributed to either increasing Gd concentration or the monoclinic to cubic structural phase change that also accompanies increased doping levels [12]. To better assess the Gd 4f interaction with the oxygen nearest neighbors, it is essential to compare the n-type Gd-doped HfO_2 with n-type Gd_2O_3, as both are in the monoclinic phase when grown on Si(100) by pulsed laser deposition. Although Gd is expected to be a p-type dopant in HfO_2, one can fabricate a heterojunction diode of n-type Gd-doped HfO_2 with silicon by overcompensating the Gd acceptor states by donor states introduced by oxygen vacancies at the lower Gd doping levels [12, 15]. This formation of donor states should more easily accomplished with Gd_2O_3.

2. Experimental details

The Gd-doped (3 at.%) HfO_2 films were deposited on single crystal silicon (100) p-type (and n-type) substrates using pulsed laser deposition (PLD) at a growth rate of about 0.15 Å s^{-1}. (Here, x% Gd means the nominal composition $Hf_{1-x}Gd_xO_{2-0.5x}$.) The Gd-HfO_2 target was prepared by standard ceramic techniques using HfO_2 and Gd_2O_3 powders,

as described elsewhere [15, 16]. The Gd_2O_3 was grown on Si(100) using a pure Gd_2O_3 target. Before the deposition, the Si(100) substrates were cleaned with diluted HF acid, rinsed with acetone, and then immediately put in vacuum chamber. Before deposition, the surface of the Si wafer was sputter cleaned in a plasma of H_2 (8%) and Ar (92%) mixture created by a DC sputtering gun operating in the reverse bias mode. The films were deposited at a substrate temperature of 500 °C. The chamber was pumped to a base pressure of 3×10^{-7} Torr and the deposition was carried out in a mixture of H_2 and Ar (8% H_2) to introduce the necessary oxygen vacancies. The vacuum was maintained at 10^{-5} Torr during the deposition. The doping level was determined from the target composition, with companion measurements using near edge x-ray absorption spectroscopy (NEXAFS), and on separate samples by x-ray emission spectroscopy (XES or EDAX) on similarly prepared samples. The complementary spectroscopies show that the films and the target have essentially the same composition.

We fabricated several diodes to illustrate the n-type band offset of the Gd_2O_3 and 3% Gd-doped HfO_2 relative to p-type silicon. The heterojunction of Gd_2O_3 and Gd-doped HfO_2 with p-type silicon forms an excellent diode, as shown in figure 1. While these data do not conclusively show the dominant carrier, they suggest that oxygen vacancies can overcompensate the Gd acceptor states in 3% Gd-doped HfO_2 without completely destroying the semiconductor properties, consistent with the photoemission [12, 15]. On n-type silicon, the heterojunctions do not show clear diode rectification and the $I(V)$ characteristics are more representative of a resistor, consistent with the picture of oxygen vacancies.

To determine the placement of the Fermi level, angle-resolved photoemission experiments were performed using the 3 m toroidal grating monochromator (3 m TGM) beam line [17] in a UHV chamber previously described [13, 14, 17]. The Fermi level (E_F) was established from a gold film in electrical contact with the sample and measurements were carried out at ambient temperatures.

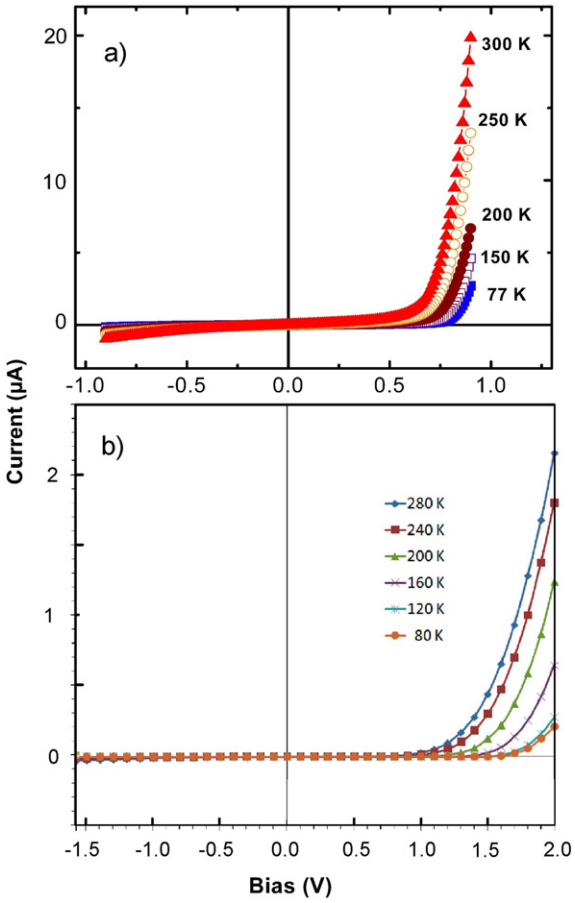

Figure 1. Current voltage characteristics for heterojunction diodes constructed from Gd-doped HfO_2 on p-type silicon (a), and from monoclinic Gd_2O_3 on p-type silicon (b), as a function of temperature. These data demonstrate the diode characteristics over a range of temperatures.

3. The structure of the films

Both x-ray diffraction and extended x-ray adsorption fine structure spectroscopy show that 3% Gd-doped HfO_2 films and Gd_2O_3 films grown on Si(100) are highly textured. As noted elsewhere [12, 15], the x-ray diffraction patterns show that the resulting approximately 250 nm thick 3% Gd-doped HfO_2 films are in a single monoclinic phase with strong texture growth, with about 3% strain compared with the undoped HfO_2 (figure 2). From the largest peak near 28° (2θ), it is estimated that the lattice spacing for $\langle\bar{1}11\rangle$ is increased by $d = 0.0030$ nm, from 0.3147(1) nm for the undoped HfO_2 films to 0.3177(1) nm for Gd-doped samples (figure 2). The peak is shifted to lower angles by 0.338°.

Gd L3 edge x-ray adsorption near edge structure (XANES) and extended x-ray absorption fine structure (EXAFS) spectra of 3% doped sample were collected at the DCM beamline at the Center for Microstructures and Devices (CAMD). Monochromatic light was obtained by using a double crystal monochromator of Lemonnier type [18], equipped with a Ge(220) crystal pair. The energy resolution was approximately 2 eV and spectra were acquired in the fluorescent yield mode, using a Ge detector (Canberra). Magnitude and imaginary part of the Fourier transformed (FT) $k\chi(k)$ of the Gd L_3 edge for 3% samples is shown in figure 3. While the magnitude of the Fourier transformed $k\chi(k)$ is not precisely the pair radial distribution function, this does provide an indication of the radial spacing of atoms in the vicinity of Gd. The first peak at ~0.8–2.5 Å corresponds to the single-scattering contribution of Gd–O pairs. A multi-peak structure at ~2.5–5.2 Å is due to combined contributions of Gd–O, and Gd–Hf single-scattering paths as well as several multiple-scattering paths, as summarized in figure 4. In other words, we find that Gd occupies the Hf site in HfO_2, consistent with expectations [12, 15].

For Gd_2O_3, the x-ray diffraction is consistent with highly textured monoclinic Gd_2O_3, not the more expected cubic structure [19, 20]. But the substrate has a strong influence on the texture and crystal structure of the Gd_2O_3 film [21, 22], as is clearly the case here. The textured structure is such that the $\langle\bar{4}02\rangle$ planes mostly lie along the surface of the film. Some (401) and (202) planes are also found to orient parallel to the surface of the film. Only the ($h0l$) planes (planes parallel to the

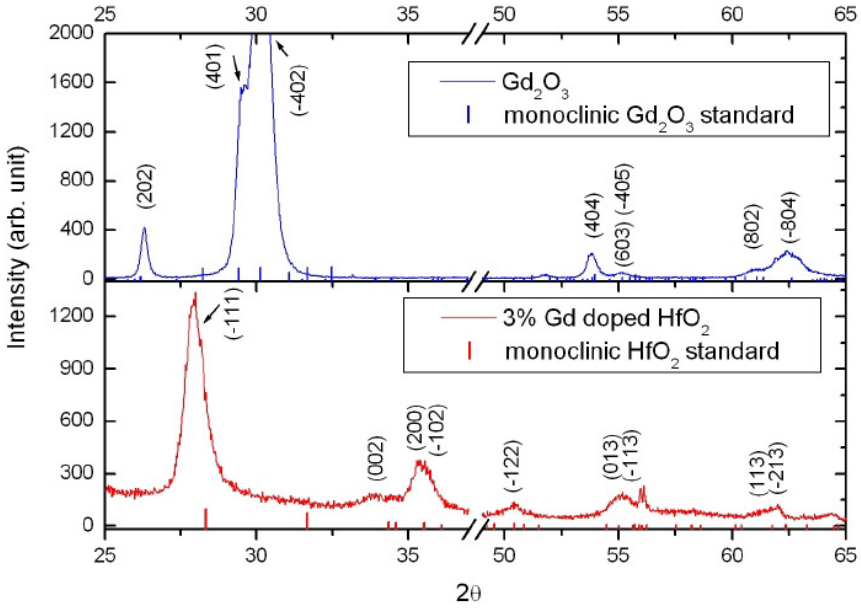

Figure 2. Part of the XRD pattern of the film is shown in figure. X-ray diffraction patterns of PLD grown Gd_2O_3 (upper panel) and 3% Gd-doped HfO_2 (lower panel). The bar diagrams included in each panel are the standards of monoclinic Gd_2O_3 and HfO_2, respectively. For 3% Gd-doped HfO_2 (lower panel), the XRD is consistent with that of HfO_2 in a simple monoclinic structure. From the largest peak near 28° (2θ), shown here, we estimated that the lattice spacing for $\langle \bar{1}11 \rangle$ is increased by $d = 0.0030(1)$ nm. The peak is shifted to lower angles by 0.338°.

(This figure is in colour only in the electronic version)

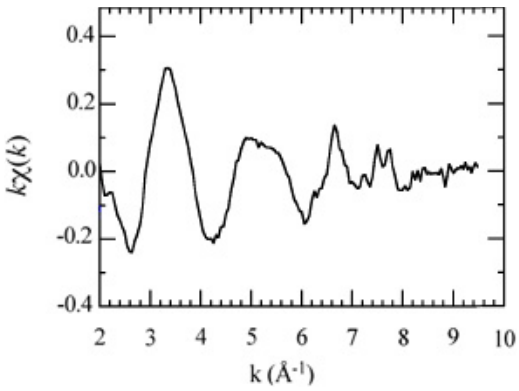

Figure 3. The $k\chi(k)$ of 3% Gd-doped HfO_2 extracted from the Gd L_3-edge EXAFS spectra.

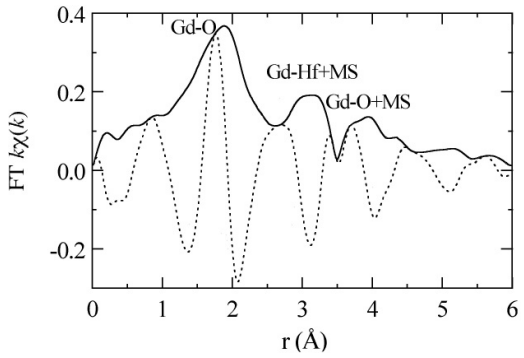

Figure 4. The Fourier transform (FT) of 3% Gd-doped HfO_2 EXAFS data. The oscillating curve (dashed lines) is the imaginary part of the Fourier transform of the data. The envelope (solid lines) are the magnitudes of the Fourier transform. The 3% data are transformed with a square window between 2.8 and 9.4 $Å^{-1}$. The peak assignment is based on HfO_2.

b axis) are grown parallel to the surface. The lattice spacing along the $\langle \bar{4}02 \rangle$ direction is about 0.2965 nm and the lattice spacing for $\langle 401 \rangle$ and $\langle 202 \rangle$ is 0.3033 nm and 0.3402 nm, respectively. The Gd_2O_3 unit cell is large with inequivalent Gd (three) and oxygen atoms (in a number of inequivalent sites) as schematically shown in figure 5. The repeat along the surface normal is eight times the $\langle \bar{4}02 \rangle$ layer spacing or about 2.372 nm.

4. The occupied density of states

From figure 6, it is clear that the valence band edge is placed well away from the Fermi level for both 3% Gd-doped and undoped HfO_2 films. As reported previously [12, 15], the Hf 4f binding energies and valence band edge are similar [23] or slightly larger than those reported elsewhere [24–26]. The shoulder on the broad photoemission peak is at the binding energy of 9–10 eV, which has been already assigned strong Gd 4f weight [12, 15].

The valence band density of states, as determined by photoemission for Gd_2O_3, are very similar to that observed for 3% Gd-doped films, as indicated in figure 7. The major difference is that for Gd_2O_3, we require four components at a minimum to fit the valence band spectra, as also indicated in figure 7. This might be expected as from the crystal structure

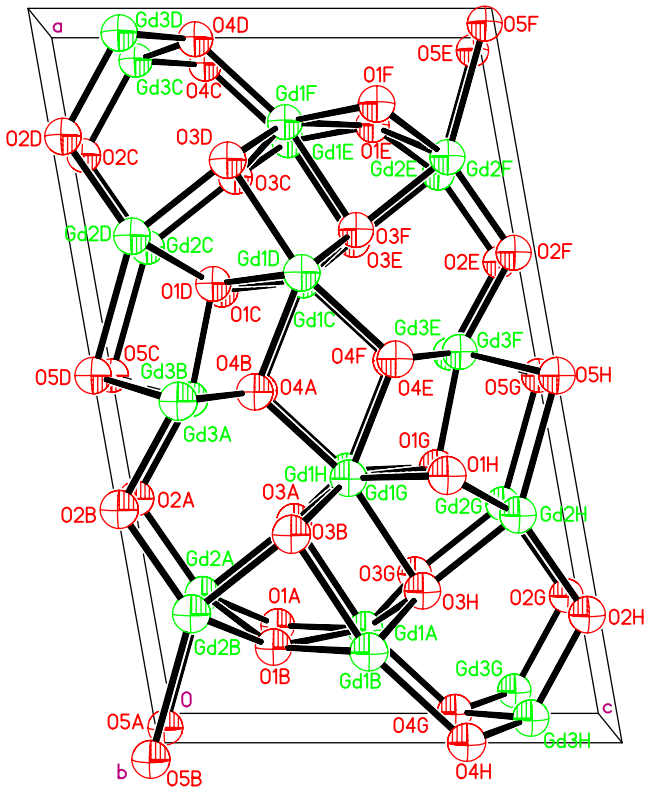

Figure 5. Structure of Gd_2O_3, with the packing of the ions in Gd_2O_3 as viewed along the *b*-axis. The green and red spheres represent gadolinium and oxygen atoms respectively. The Gd $\cdots$ Gd interactions are not shown.

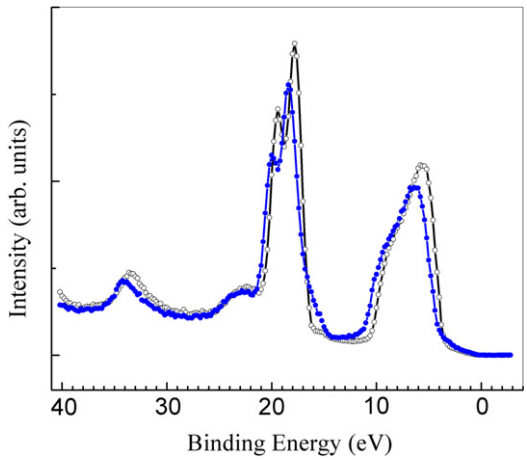

Figure 6. Different bands intensities for pristine (open dots) and Gd-doped films of HfO_2 (filled blue dots). The photon energy is 100 eV and the light incidence angle is 45°. All photoelectrons were collected along the surface normal at $T = 320\,^{\circ}\mathrm{C}$.

as there are differences in the crystal field around oxygen and gadolinium: there are two very inequivalent oxygen species, and to a lesser extent true as well of gadolinium, as indicated in figure 5. In fact the gadolinium atoms occupy three inequivalent sites as well, but this does not really lead to a further splitting in the valence band electronic structure sufficient to explain, as discussed below, the two widely separated Gd 4f components at a binding energy of about 8.7–

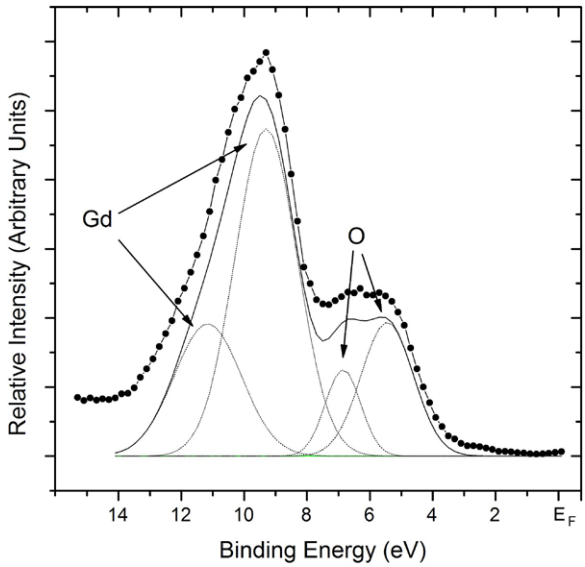

Figure 7. The photoemission spectrum of the valence band $Gd_2O_3\,\langle\bar{4}02\rangle$. The various components contributing to the valence band structure are indicated, and major contributions to the photoemission features indicated. The photon energy is 117 eV and the light incidence angle is 45°. All photoelectrons were collected along the surface normal at $T = 240\,^{\circ}\mathrm{C}$.

9.5 eV below the Fermi level and the 'shoulder' at a binding energy of 11–12 eV.

Confirmation that the Gd 4f states contribute to the shoulder at 9–10 eV on the broad photoemission feature from 5 to 10 eV binding energy is found in resonant photoemission (i.e. constant initial state spectroscopy) measurements of Gd-doped HfO_2. The results are shown in figure 8. The photoelectron intensities from Gd-doped HfO_2, determined from the feature at about 9.5 eV binding energy (from the Fermi level) is strongly enhanced at about 149 eV photon energy. Similarly for Gd_2O_3, we see that the components of the valence band at about 8.7–9.5 eV and the 'shoulder' at 11–12 eV binding energies are enhanced at about 152 eV, as shown in figure 9 and plotted in figure 10. For comparison, we have plotted this resonant enhancement in the valence band photoemission spectra, for both Gd_2O_3 and Gd-doped HfO_2 films for various photon energies in figures 10(a) and (b) respectively.

It is clear that the resonant enhancements in the photoemission intensity, from this 9.5 eV binding energy final state for Gd-doped HfO_2 and 8.7–9.5 eV for Gd_2O_3, occur at photon energies corresponding to the core threshold binding energy of the Gd $4d_{3/2}$ (147 eV) shallow core although at somewhat larger photon energy for Gd_2O_3. This shift of the photoemission resonance to higher photon energies is expected because of the increase in binding energy of the 4d core and decrease in the conduction band edge binding energy (a placement of the conduction band edge well above the Fermi level [26]). These are in these nominally dielectric oxides, as compared to gadolinium metal. Thus the feature, in the region of 9.5 eV binding energy final state for Gd-doped HfO_2 and 8.7–9.5 eV for Gd_2O_3, has strong Gd weight. The resonant photoemission process occurs because of an excitation from

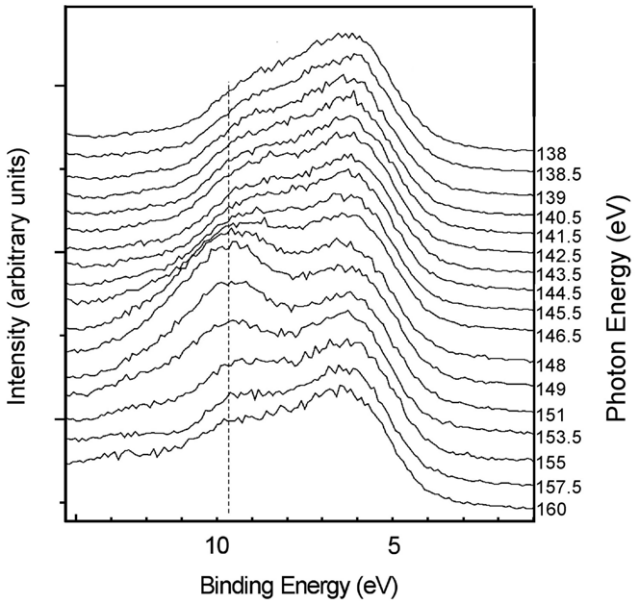

Figure 8. Resonant photoemission spectra for photon energies through the 4d → 4f resonance for Gd-doped films of HfO_2. Light incidence angle is 45°. All photoelectrons were collected along the surface normal.

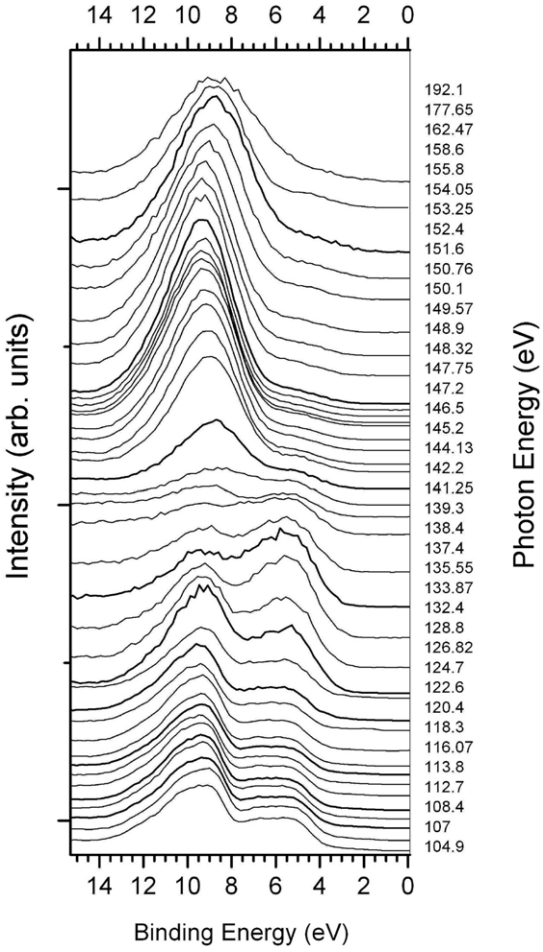

Figure 9. The resonant photoemission spectra for photon energies through the 4d → 4f resonance for Gd_2O_3. Light incidence angle is 45°. All photoelectrons were collected along the surface normal.

the 4d cores to a bound state, but with a final state identical to that resulting from direct photoemission from Gd 4f states [27–29]. The photoemission resonance, with changing photon energy, is due to constructive interference between the direct 5f photoionization and a $4d^{10}\ 4f^7 \rightarrow 4d^9\ 4f^8 \rightarrow 4d^{10}\ 4f^6 + e^-$ super Coster–Kronig transition [28], leading to a classic Fano resonance. The classic Fano resonance shape is very clearly seen for the Gd 4f weighted valence band feature intensities, as plotted in figure 10(a).

These results are generally in agreement with our expectations from the calculated band structure and density of states. The electronic structure of the B-type Gd_2O_3 (monoclinic) having six formulae units per monoclinic cell has been calculated using the projected augmented wave method and the generalized gradient approximation (GGA-PBE) with Hubbard U correction (GGA + U) [30] on the Gd 4f energy levels, as implemented in the VASP package [31]. In the GGA + U calculations, we used $U = 7.5$ eV and $J = 0.6$ eV for the Gd 4f orbitals to take the correlation effects into account. The value of the Hubbard U used here is very close to the value used for the Gd 4f energy levels in the molecular endo-fullerene Gd@C_{60} [29]. A similar (although somewhat smaller) value of $U = 6.7$ eV was found to be appropriate in the examples of the Gd pnictides GdX (X = N, P, As, and Bi) compounds [32].

The calculated value of the band gap for the B-type Gd_2O_3 (monoclinic) from the GGA + U method is 3.8 eV. The monoclinic Gd_2O_3 density of states (DOS), broadened with a Gaussian width 0.2 eV, is shown in figure 11. The total density of states has been projected onto each atomic species (gadolinium and oxygen) showing the strong Gd 4f character at the DOS peak around $E = -6.3$ eV and the major oxygen 2p character over the energy range of −5 to 0 eV. This calculation places the occupied Gd 4f levels are a binding energy slightly greater (by about 0.5–1 eV), relative to the valence band maximum, than is observed in experiment, even if only the major Gd 4f component is considered.

There are three different Gd sites Gd(1), Gd(2) and Gd(3) in monoclinic Gd_2O_3, with different coordination numbers and neighboring atoms. To analyze the Gd 4f DOS peak, we calculated the contributions of crystallographically different Gd atoms (figure 5) to the DOS, as indicated by Gd(1), Gd(2), and Gd(3) in the inset of figure 11. While there are clearly differences between Gd(1) and Gd(3), there are some similarities. Each Gd atom site has seven oxygen neighbors, however, for Gd(3), the seventh oxygen neighbor is located farther away than for Gd(1) and Gd(2), so only six neighbor are included in the primary coordination shell. The coordination about Gd(3) is a distorted octahedron with the seventh oxygen atom along a three-fold axis. For Gd(1) and Gd(2), this is not the case, and both have the same 2*mm* symmetry and seven oxygen neighbors within the primary coordination shell (figure 5). The six oxygen about Gd(1), or Gd(2), form a trigonal prism and the seventh lies along a normal to a prism face. In considering the Gd–Gd distances, Gd(1) and Gd(2) are again similar, having 10 Gd neighbors at distances ranging from 3.28 to 3.98 Å and two more Gd atoms placed further

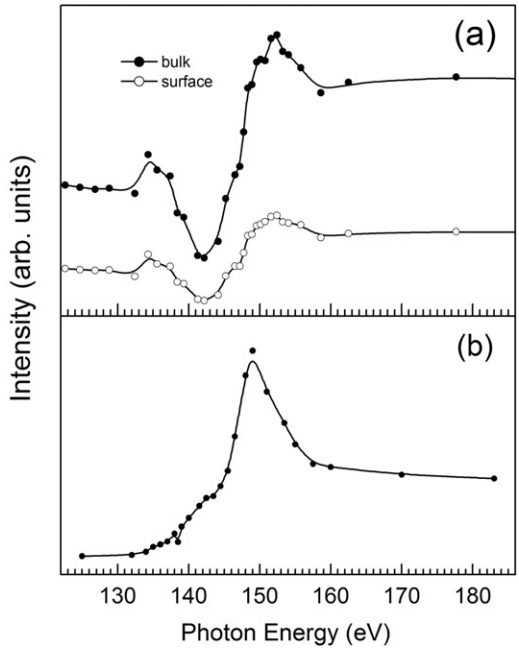

Figure 10. The resonant photoemission intensities through the 4d → 4f resonance for Gd_2O_3 (a) and Gd-doped films of HfO_2 (b), abstracted from figures 8 and 9. For Gd_2O_3, there are seen to be two Gd 4f components at a binding energy of about 8.7–9.5 eV below the Fermi level and the 'shoulder' at a binding energy of 11–12 eV, which are assigned as bulk (–●–) and surface (–○–) components respectively (see text).

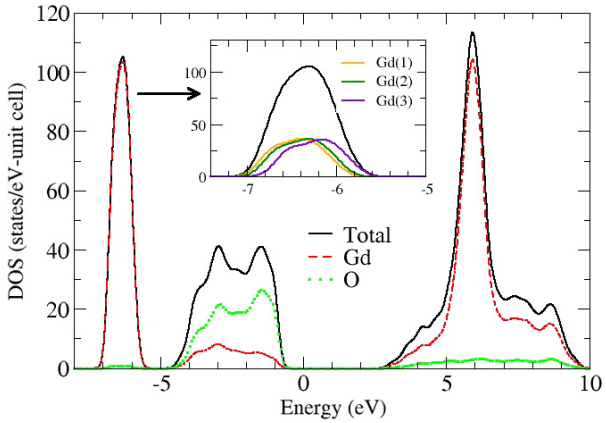

Figure 11. The calculated density of states for monoclinic (type B) Gd_2O_3. The monoclinic Gd_2O_3 density of states (DOS) has been broadened with a Gaussian width 0.2 eV. The total density of states has been projected onto each atomic species (gadolinium and oxygen) showing the strong Gd 4f character at the DOS peak around $E = -6.3$ eV and the major oxygen 2p character hybridized with Gd 5d orbitals over the energy range of −5 to 0 eV.

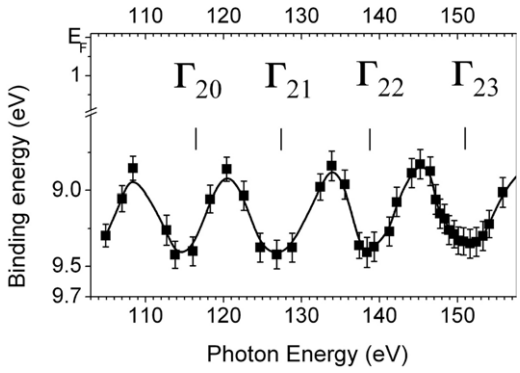

Figure 12. The dispersion of the Gd 4f component, with changing photon energy. The critical points are indicated, assuming no inner potential and the predicted lattice spacing of 23.7 Å along ⟨4̄02⟩.

away. On the other hand, Gd(3) has 12 Gd neighbors ranging from 3.58 to 3.87 Å.

As a result, the Gd 4f DOS peak originates from the three distinct types of Gd atoms whose corresponding 4f energy levels are split by as much as ∼0.5 eV due to the spin–orbit coupling but are rigidly shifted due to their crystallographic identities. The full linewidth of the Gd 4f DOS peak is about 1.3 eV.

Since the two components we have identified in photoemission of $Gd_2O_3\langle\bar{4}02\rangle$ as heavily Gd 4f, in weight or oscillator strength (on the basis of their photon energy dependence at the $4d^{10}\ 4f^7 \rightarrow 4d^9\ 4f^8 \rightarrow 4d^{10}\ 4f^6 + e^-$ super Coster–Kronig transition, shown in figure 10(a)), are separated by slightly more than 2 eV, we must conclude that the higher binding energy component is, in fact, a consequence of the surface-to-bulk shift. The Gd occupied 4f surface-to-bulk shift is only about 0.4 eV for Gd metal, but is expected to be much larger with oxidation [33, 34], with the surface component at the greater binding energy. Both exhibit very similar resonance It is the larger intensity component, at 8.7–9.5 eV binding energy, associated with the bulk Gd 4f weighted bands of Gd_2O_3, that are of interest in establishing the occupied Gd 4f band structure.

5. The 4f band structure of gadolinium oxide

Because of the high degree of order and the strong texture growth along ⟨4̄02⟩, we have been able to measure the bulk band structure along ⟨4̄02⟩. Because the photoelectrons are collected along the surface normal in the sequence of photon energy dependent photoemission spectra (figure 9), the binding energy shifts of many of the observed photoemission features is indicative of band dispersion along the electron wave vector normal to the surface, $k_\perp$. The value of $k_\perp$ can be estimated from the photoelectron kinetic energy making some assumptions about the inner potential U_{in}:

$$k_\perp = \sqrt{\frac{2m}{\hbar^2}\{E_{\text{kin}}(\cos(\theta))^2 + U_{\text{in}}\}}. \qquad (1)$$

The dispersion of the component we attribute to the Gd 4f level at 9–9.5 eV binding energies is summarized in figure 12. The dependence on photon energy shows that the 4f band critical points repetition, whose spacing in wave vector suggests a periodicity of about 22 ± 2 Å perpendicular to the film or along the surface normal, close to the value of 23.72 Å expected from the crystallography.

For a dielectric insulator we would expect that the value of the inner potential to be effectively negligible, as seems to be the case here. We cannot establish that the inner potential to be zero, but from our measurements, that establishes the critical points for the 19th through to the 23rd Brillouin zone, the inner potential is quite small and is no more than 1–2 eV, at most. Assuming a value of zero for the inner potential, and a lattice constant of 23.72 Å, the calculated critical points show very good agreement with the experimental band structure, as indicated in figure 12.

What is clear is that we have strong Gd 4f hybridization with the oxygen in both Gd_2O_3 and Gd-doped HfO_2 films, and we have a small amount of band dispersion in the band strongly weighted with a Gd 4f contribution for Gd_2O_3. The band dispersion is small (about 500 meV), but evident nonetheless, as in the case of Ce [2, 3] and Yb [4] compounds. The Gd 4f weighted bands exhibits band structure yet are placed well away from the Fermi level in the valence band of Gd_2O_3.

The band width is about 0.5 eV, which is less than the full Gd 4f linewidth in Gd_2O_3, but nonetheless about what is expected from the calculated band width from projected augmented wave method and the generalized gradient approximation (GGA-PBE) with a Hubbard U correction (GGA + U). What is perhaps surprising is that that we are able to identify this band structure experimentally even though there are some 84 gadolinium bands. This implicates that photoemission selection rules play a role. Such selection rules are indeed likely.

The unoccupied 4f levels of Gd_2O_3 also have some band width. From the width of the resonant intensities due to the $4d^{10}\ 4f^7 \rightarrow 4d^9\ 4f^8 \rightarrow 4d^{10}\ 4f^6 + e^-$ super Coster–Kronig transition occurring at about 150–152 eV, we can see that the width of this resonant enhancement occurs for a far larger range of photon energies for Gd_2O_3 than is the case for 3% Gd-doped HfO_2 (figures 10(a) and (b) respectively). Since Gd_2O_3 and HfO_2 have very similar band gaps (5.4 and 5.7 eV respectively), the pronounced differences in the position of the maximum resonance and the width of the resonance suggest that the unoccupied Gd 4f bands of Gd_2O_3 have greater band width than is the case for the unoccupied states of Gd in HfO_2. As was noted for ErAs [13, 14], we expect the unoccupied 4f levels to exhibit dispersion and contribute to the band width of the unoccupied states.

6. Conclusion

In summary, we find that superficially there are many similarities in the valence band electronic structure of monoclinic Gd-doped HfO_2 and monoclinic Gd_2O_3. We find that with Gd_2O_3, there is a surface-to-bulk shift of the Gd 4f levels in Gd_2O_3, not seen with Gd-doped HfO_2, but treating the Gd 4f levels as shallow core levels may not be appropriate. We find that in spite of the high index face adopted by Gd_2O_3 thin films on Si(100), and the large unit cell of Gd_2O_3, Gd 4f band structure is nonetheless and perhaps surprisingly apparent.

Acknowledgments

The authors acknowledge insightful discussions with David Wisbey, Alex Ignatov, Andre Petukhov, and J Brand. The authors would like to thank Bryan Blasey, LTC David LaGraffe, and A Ignatov for their technical help with some of the measurements. This work was supported by the Office of Naval Research (Grant No. N00014-06-1-0616), the Defense Threat Reduction Agency (Grant No. HDTRA1-07-1-0008 and MIPR 06-2310M), and the Nebraska Research Initiative. This work was undertaken in partial fulfilment of the degree at AFIT by one author (DW). The views expressed in this paper are those of the authors and do not reflect the official policy or position of the Air Force, Department of Defense or the US Government.

References

[1] Olson C G, Chase S J, Canfield P and Lynch D W 1998 *J. Electron Spectrosc. Relat. Phenom.* **93** 175
[2] Im H J, Ito T, Kim H D, Kimura S, Lee K E, Hong J B, Kwon Y S, Yasui A and Yamagami H 2008 *Phys. Rev.* B **100** 176402
[3] Andrews A B, Joyce J J, Arko A J and Fisk Z 1996 *Phys. Rev.* B **53** 3317
[4] Vyalikh D V, Danzenbacher S, Yaresko A N, Holder M, Kucherenko Y, Laubschat C, Krellner C, Hossain Z, Geibel C, Shi M, Patthey L and Molodtsov S L 2008 *Phys. Rev. Lett.* **100** 056402
[5] Guziewicz E, Durakiewicz T, Butterfield M T, Olson C G, Joyce J J, Arko A J, Sarrao J L, Moore D P and Morales L 2004 *Phys. Rev.* B **69** 045102
[6] Guziewicz E, Durakiewicz T, Oppeneer P M, Joyce J J, Thompson J D, Olson C G, Butterfield M T, Wojakowski A, Moore D P and Arko A J 2006 *Phys. Rev.* B **73** 155119
[7] Arko A J, Joyce J J, Andrews A B, Mandrus D, Moshopoulou E, Fisk Z and Canfield P C 1997 *Phil. Mag.* B **75** 603
[8] Roy L E, Durakiewicz T, Martin R L, Peralta J E, Scuseria G E, Olson C G, Joyce J J and Guziewicz E 2008 *J. Comput. Chem.* **29** 2288
[9] Guziewicz E, Durakiewicz T, Olson C G, Joyce J J, Butterfield M T, Arko A J, Sarrao J L and Wojakowski A 2006 *Surf. Sci.* **600** 1632
[10] Molodtsov S L, Boysen J, Richter M, Segovia P, Laubschat C, Gorovikov S A, Ionov A M, Prudnikova G V and Adamchuk V K 1998 *Phys. Rev.* B **57** 13241
[11] Sabirianov R F, Mei W N, Lu J, Gao Y, Zeng X C, Bolskar R D, Jeppson P, Wu N, Caruso A N and Dowben P A 2007 *J. Phys.: Condens. Matter* **19** 082201
[12] Losovyj Ya B, Ketsman I, Sokolov A, Belashchenko K D, Dowben P A, Tang J and Wang Z 2007 *Appl. Phys. Lett.* **91** 132908
[13] Komesu T, Jeong H-K, Choi J, Borca C N, Dowben P A, Petukhov A G, Schultz B D and Palmstrøm C J 2003 *Phys. Rev.* B **67** 035104
[14] Duan C-G, Komesu T, Jeong H-K, Borca C N, Yin W-G, Liu J, Mei W N, Dowben P A, Petukhov A G, Schultz B D and Palmstrøm C J 2004 *Surf. Rev. Lett.* **11** 531–9
[15] Ketsman I, Losovyj Ya B, Sokolov A, Tang J, Wang Z, Belashchenko K D and Dowben P A 2007 *Appl. Phys.* A **89** 489–92
[16] Wang W, Hong Y, Yu M, Rout B, Glass G A and Tang J 2006 *J. Appl. Phys.* **99** 08M117

[17] Losovyj Ya B, Ketsman I, Morikawa E, Wang Z, Tang J and Dowben P 2007 *Nucl. Instrum. Methods Phys. Res.* A **582** 264–6
[18] Lemonnier M, Collet O, Depautex C, Esteva J M and Raoux D 1978 *Nucl. Instrum. Methods* A **152** 109
[19] Haire G and Eyring L 1994 *Handbook on the Physics and Chemistry of Rare Earths* vol 18 (London: Elsevier) p 429
[20] Horosaki N, Ogata S and Kocer C 2003 *J. Alloys Compounds* **351** 31
Gila B P, Lee K N, Johnson W, Ren F, Abemathy C R, Pearton S J, Hong M, Kwo J, Mannaerts J P and Anselm K A 2000 *IEEE Trans.* vol IV-1, p 182
[21] Hong M, Kwo J, Kortan A R, Mannaerts J P and Sergent A M 1999 *Science* **283** 1897
[22] Yacoby Y, Sowwan M, Stern E, Cross J O, Brewe D, Pindak R, Pitney J, Dufresne E M and Clarke R 2002 *Nat. Mater.* **1** 99
[23] Komatsu M, Yasuhara R, Takahashi H, Toyoda S, Kumigashira H, Oshima M, Kukuruznyak D and Chikyow T 2006 *Appl. Phys. Lett.* **89** 172107
[24] Suzer S, Sayan S, Banaszak Holl M M, Garfunkel E, Hussain Z and Hamdan N M 2003 *J. Vac. Sci. Technol.* A **21** 106
[25] Sayan S, Emge T, Garfunkel E, Zhao X, Wielunski L, Bartynski R A, Vanderbilt D, Suehle J S, Suzer S and Banaszak Holl M M 2004 *J. Appl. Phys.* **96** 7485
[26] Sayan S, Bartynski R A, Zhao X, Gusev E P, Vanderbilt D, Croft M, Banaszak Holl M M and Suzer S 2004 *Phys. Status Solidi* b **241** 2246
[27] Dowben P A, Li D, Zhang J and Onellion M 1995 *J. Vac. Sci. Technol.* A **13** 1549
[28] Kachel T, Rochow R, Gudat W, Jungblut R, Rader O and Cabone C 1992 *Phys. Rev.* B **45** 7276
[29] Sabirianov R F, Mei W N, Lu J, Gao Y, Zeng X C, Bolskar R D, Jeppson P, Wu N, Caruso A N and Dowben P A 2007 *J. Phys.: Condens. Matter* **19** 082201
[30] Liechtenstein A I, Anisimov V I and Zaanen J 1995 *Phys. Rev.* B **52** R5467
[31] Kresse G and Joubert D 1999 *Phys. Rev.* B **59** 1758
[32] Duan C-G, Sabiryanov R F, Liu J, Mei W N, Dowben P A and Hardy J R 2005 *Phys. Rev. Lett.* **94** 237201
Duan C-G, Sabiryanov R F, Mei W N, Dowben P A, Jaswal S S and Tsymbal E Y 2007 *J. Phys.: Condens. Matter* **19** 315220
[33] McIlroy D N, Waldfried C, Li D, Pearson J, Bader S D, Huang D-J, Johnson P D, Sabiryanov R F, Jaswal S S and Dowben P A 1996 *Phys. Rev. Lett.* **76** 2802–5
[34] Schussler-Langeheine C, Meier R, Ott H, Hu Z, Mazumdar C, Grigoriev A Y, Kaindl G and Weschke E 1999 *Phys. Rev.* B **60** 3449–52